

One Leaf Knows Autumn: A Piece of Data-Model Facilitates Efficient Cancer Prognosis with Histological and Genomic Modalities

Anonymous authors

Paper under double-blind review

Abstract

The rapidly emerging field of computational pathology enables integrated image-omic solutions for cancer prognosis by jointly modeling both histological and genomic data. However, current multi-modal techniques suffer from three major bottlenecks: (1) Memory Overheads, since a raw histology image typically has a super high resolution, e.g., $203,183 \times 91,757$ in cancer HNSC. Simple patch partitioning trades training time for spaces. (2) Massive Computing Costs, due to immense parameter counts in recent state-of-the-art models, which demand substantial computational resources. Meanwhile, their intrinsic representation redundancy in vanilla-trained networks leads to an ineffective usage of the capacity. (3) Gradient Conflicts, because there are significant heterogeneities between image and genomic data modalities, resulting in the disagreement of optimization directions. In this work, we propose an effective multi-modal pipeline for cancer prognosis, i.e., **CancerMoE**, to address the aforementioned challenges. Specifically, from data to model, it first designs a dynamic patch selection algorithm to flexibly score and locate informative patches online, trimming down the memory cost; then introduces a Sparse Mixture-of-Experts (SMoE) framework to disentangle weight spaces and allocate the most relevant model pieces to an input sample, promoting training efficiency and synergistic optimization among multiple modalities; finally, consolidates and scarifies redundant attention heads, leading to improved efficiency and interpretability. Our extensive experiments demonstrate that **CancerMoE** achieves competitive performance on **twelve** cancer datasets compared to previous methods. Meanwhile, our proposed network architecture requires only **1%** of the image patches, **20%** of the model parameters, and **30%** of the merged attentions compared with the vanilla transformer network. Key codes are provided in detail in the supplement.

1 Introduction

In cancer research, a comprehensive examination of various facets is often needed to unravel the intricate nature of this complex disease Marusyk & Polyak (2010); Marusyk et al. (2012). Prognosis Sala et al. (2017); Thakor & Gambhir (2013) serves as one of the promising approaches to develop an understanding of cancer and predict the survival chance of patients, equipping with cutting-edge technologies like molecular profiling Yanaihara et al. (2006), imaging modalities Shahbazi-Gahrouei et al. (2019), and genetic analysis Kamps et al. (2017); Claus et al. (1991). Moreover, the joint investigation between tumor microenvironments (*e.g.*, histological images) and its interplay with immune responses (*e.g.*, genomic profiles) sheds light on the intrinsic dynamics that influence tumor development and metastasis Heindl et al. (2015); Kather et al. (2018); Tarantino et al. (2021), paving the way for effective survival prediction and further treatment.

Specifically, the advent of high-throughput sequencing technologies has brought about significant advances in survival analysis, leading to a shift from the sole examination of clinical indicators to the integration of genomic profiles with pathological images. Recent investigations Shimizu et al. (2022); Gobin et al. (2019); Kalra et al. (2020); Mayekar & Bivona (2017); Zhang et al. (2022); Lu et al. (2022) have highlighted the benefits of exploring multi-modal analysis. Unfortunately, current learning-based integration solutions are

still in the initial stage of fusing multi-modal knowledge in a straightforward way. For instance, Braman et al. (2021); Cheerla & Gevaert (2019); Chen et al. (2020) directly combine pathological features and genomic profiles for survival prediction, which overlook inherent cross-modal interactions; Li et al. (2021); Wang et al. (2021); Chen et al. (2021b) utilize genomic embeddings to guide the attention aggregation of pathological image features, disregarding information that may not be associated with gene expressions. Thus, there is an immediate demand for an effective integration mechanism adept at deciphering the domain-specific heterogeneity within histological and genomic data modalities. Concurrently, while recent advancements in learning algorithms have shown promising performance that surpasses human experts, their demanding computational cost poses significant challenges to scalability and practical application.

In light of this, our paper targets effective integration, aiming to address computing bottlenecks in three intertwined aspects. ① *Memory Overheads*. Histology images usually have super high resolutions, *e.g.*, $191,352 \times 91,562$ in cancer LUAD and $139,008 \times 256,256$ in cancer BRCA, which require substantial CPU/GPU memories to load and process the data. A conventional way is segmenting the high-resolution images and creating millions of smaller patches Kong et al. (2023); Dosovitskiy et al. (2020). However, it actually trades longer training time for memory reductions. ② *Training Efficiency*. Millions of patches and huge parameter counts in recent State-of-the-Art (SoTA) transformer-based models Chen et al. (2022a) severely question the resource intensity during training. ③ *Inference Efficiency*. Another efficiency concern and drawback lies in the insufficient utilization of model capacity. As presented in recent studies Yuan et al. (2021); Gao et al. (2021); He et al. (2023), only a small portion of network weights, like 5% Zhang et al. (2021); Allen-Zhu & Li (2019) of total parameter counts, are engaged during the inference of each sample. A few pioneering efforts have explored dynamic sparsity as initial remedies, to cut redundancy and boost training and inference efficiency.

To overcome the aforementioned challenges in terms of effective integration and efficient computing (①+②+③), we propose a novel framework, namely, **CancerMoE**, for ultra-efficient data integration for cancer prognosis. The innovative designs span both data and model perspectives. Along with the information feedforward, it first employs a dedicated Dynamic Patch Selector (DPS) that meticulously examines and selects crucial image patches abundant in histological information, while discarding redundant ones. It significantly reduces the heavy costs associated with memory and training time. Then, a tailored SMOE architecture is invented to learn modality-specific and -agnostic modules to synergize multi-modality optimization. In detail, modularization and modality-aware routing policies are leveraged to disentangle the model parameter space and allocate input tokens to different model pieces, aiming for computational efficiency and mitigated conflicts of multi-modal gradients, respectively. Lastly, we investigate and diminish the attention redundancy by proposing the Attention Consolidation and Sparsification (ACS) mechanism. It appropriately clusters multiple attention heads and reduces superfluous attention connections, which brings improved training and inference efficiency and interpretability. Our innovation efforts can be summarized into the following four thrusts:

- ★ Given 1% patches of histological images, the same genomic profiles, and 20% model parameters, we demonstrate promising performance and efficiency for predicting the survival of cancer patients. We introduce **CancerMoE**, an effective multi-modal learner in cancer prognosis, that seamlessly integrates histology images and genomics profiles.
- ★ We design a dynamic patch selector mechanism to score and select the most crucial image patches (*e.g.*, 1% of total patches) online, which avoids loading the full-resolution image and discards its massive memory overheads.

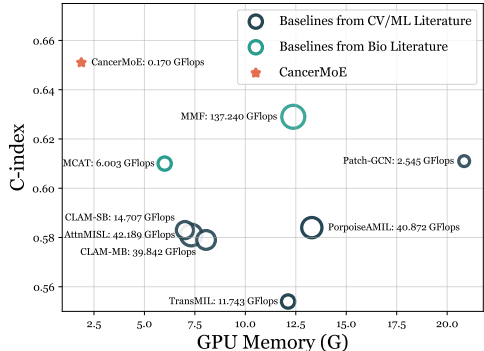


Figure 1: The performance of histology-genomic cancer prognosis on the BRCA dataset. Averaged results and the required memory cost are reported. Markers ★ and ○ denote “ours” and “baseline” approaches, respectively. A larger marker indicates more floating point operations (FLOPs) are used for inference. The top left corner implies the most ideal solution.

- ★ We propose a consolidation and sparsification algorithm for self-attention modules to reduce intrinsic redundancy and promote efficiency. It first merges insignificant attention heads into a few knowledgeable ones, then eliminates less informative elements in their attention maps.
- ★ Extensive empirical studies are conducted to validate the effectiveness of **CancerMoE** on **twelve** representative cancer datasets. Specifically, our approaches surpass the **ten** existing state-of-the-art methods by a clear performance margin of 4.1% ~ 18.2% accuracies with 8.9% ~ 31.2% memory and 0.1% ~ 2.1% FLOPs as shown in Fig. 1.

2 Related Work

Multi-Modality Learning (MML). Integrating multiple modalities of data (*e.g.*, vision, text, and audio) has a long history in the Machine Learning (ML) community Lahat et al. (2015); Bayouhdh et al. (2021); Ngiam et al. (2011); Baltrušaitis et al. (2018). The recent trend is leveraging transformer-based models as a universal backbone to enable effective multi-modal learning Ramesh et al. (2022); Saharia et al. (2022); Xia et al. (2023); Dai et al. (2022). MML also plays a crucial role in medical applications. For example, Suresh et al. (2017) merge chest X-rays, textual clinical notes, and longitudinal measurements for intensive care monitoring. Zhou & Chen (2023) design a cross-modal translation and alignment framework to capture intrinsic cross-modal correlation and discard irrelevant pathological information to gene expressions. Nowadays, along with the rapid and explosive developments of computing and AI4Medicine, there has been a surge in research efforts aimed at creating systems proficient in multimodal medical scenarios Subbiah Parvathy et al. (2020); Huang et al. (2023); Zhu et al. (2022b); Muhammad et al. (2021); Li et al. (2022). Among this huge family, Zhu et al. (2022b) propose an adaptive co-occurrence pipeline to improve the modality fusion quality through a filter-based image decomposition algorithm. Subbiah Parvathy et al. (2020) utilizes an enhanced monarch butterfly optimization to decide a better threshold of fusion rules in shearlet transform, where low and high-frequency sub-bands are fused on the basis of corresponding feature maps. Li et al. (2022) presents a hierarchical multimodal integration approach by employing a factorized bilinear model to fuse genomic and image features in a step-by-step manner.

Histology-Genomic Cancer Prognosis. Cancer prognosis involving histological images and genomic data has gained increasing popularity Chen et al. (2020); Li et al. (2022), which seamlessly combines tissue structure study with genetic data analysis. For instance, Galateau-Salle et al. (2016) explores an integrative genomics framework for constructing a prognostic model to clear renal cell carcinoma. Hao et al. (2019) introduces a biology-informed ML pipeline to identify genetic and histopathological patterns, aiming at advanced survival predictions. Mobadersany et al. (2018) shows superior prediction accuracy of patients’ overall survival. To be more specific, they create a multi-modal clinical paradigm to learn and integrate knowledge from both histology images and genomic biomarkers. Recently, numerous efforts Natrajan et al. (2016); Kather et al. (2019); Coudray et al. (2018); Subramanian et al. (2018); Mobadersany et al. (2018); Echle et al. (2021); Hou et al. (2022) have been conducted to revolutionize how we diagnose and treat cancer by jointly modeling both tissue structure (*e.g.*, pathological images) and genetic data.

Sparse Mixture-of-Experts (SMoE). The conventional dense mixture-of-experts utilizes all experts for each input sample, and therefore it is computationally demanding and expensive. Latest investigations Lepikhin et al. (2020); Shazeer et al. (2017a); Fedus et al. (2022) propose an efficient alternative, *i.e.*, SMoE, by sparsely activating a small portion of experts. Such sparse gating fashion brings substantial efficient gains in both the training and inference stages, facilitating the scaling of deep neural networks to massive sizes, *e.g.*, even to trillions of parameters Fedus et al. (2022). SMoEs have exhibited remarkable efficacy in the realms of computer vision Lou et al. (2021); Eigen et al. (2013); Riquelme et al. (2021); Ahmed et al. (2016); Gross et al. (2017); Wang et al. (2020); Abbas & Andreopoulos (2020); Pavlitskaya et al. (2020) and NLP Kim et al. (2021b); Shazeer et al. (2017a); Lepikhin et al. (2020); Zhou et al. (2022); Zhang et al. (2021); Zuo et al. (2021); Jiang et al. (2021). Several pioneering investigations take the advantage of this conditional computing nature to allocate task-relevant Ma et al. (2018); Aoki et al. (2021); Hazimeh et al. (2021); Kim et al. (2021a); Fan et al. (2022); Ye & Xu (2023); Chen et al. (2023) model pieces or modality-relevant Mustafa et al. (2022); Zhu et al. (2022a); Kudugunta et al. (2021) ones in a dynamic way for multi-task or multi-modal learning, respectively. In cancer research, a few pilot studies have been performed Raman et al. (2010); Myoung

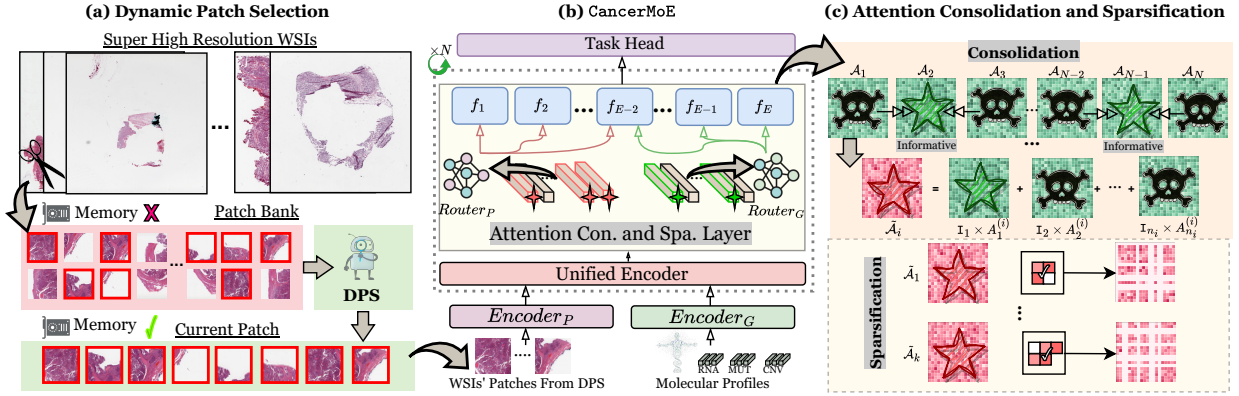


Figure 2: The entire architecture design of **CancerMoE**. The key components of this network include: (1) Dynamic Patch Selection (DPS) flexibly scores all patches in an online fashion, identifying elite patches; (2) Histopathological images and genomic data are individually transformed into embeddings and merged across modalities within a unified encoder; (3) Leveraging the Attention Consolidation and Sparsification (ACS) mechanism, the **CancerMoE** automatically filters out elements with low informational value from attention maps, selectively guiding high-quality tokens to respective experts for efficient cancer prognosis prediction.

(2013); Übeyli (2005); Kreutz et al. (2001); Afshar et al. (2021), but most investigations are limited to single modality learning and single cancer. The significant heterogeneity among modalities, memory bottlenecks gave super-high-resolution images, and diverse learning objectives led to challenging optimization issues for SMOE models and their study in cancer prognosis problems. In this regard, this paper attempts to provide an effective answer.

3 Methodology

Revisiting Sparse Mixture-of-Experts (SMoE). The SMoE pipeline typically contains a router \mathcal{R} and a group of experts $\{f_1, f_2, \dots, f_E\}$, where E is the number of experts. The output representation is then calculated by $\mathbf{y} = \sum_{i=1}^E \mathcal{R}(\mathbf{x})_i \cdot f_i(\mathbf{x})$, where $f_i(\mathbf{x})$ denotes the intermediate feature produced by expert f_i and a weighted summation is performed based on their coefficients $\mathcal{R}(\mathbf{x})_i$. Specifically, the router function is described as $\mathcal{R}(\mathbf{x}) = \text{TopK}(\text{softmax}(g(\mathbf{x})), k)$, where \mathcal{R} activates the top- k expert networks with the largest scores $g(\mathbf{x})$ given an input embedding \mathbf{x} . Also, g is a learnable neural network, as a Multi-Layer Perception (MLP). Meanwhile, the TopK function is shown as:

$$\text{TopK}(\mathbf{v}, k) = \begin{cases} \mathbf{v} & \text{if } \mathbf{v} \text{ is in the top } k \\ 0 & \text{otherwise} \end{cases}, \quad (1)$$

which preserves the largest k values in \mathbf{v} and sets the rest of the elements to zero.

Revisiting Self-Attention. In the classic design of a self-attention mechanism, input tokens $\{p_i\}_{i=1}^L, p_i \in \mathbb{R}^{d \times 1}$ are fed into three linear layers to produce the query \mathcal{Q} , key \mathcal{K} , and value \mathcal{V} matrices, respectively. Each output matrix, $\mathcal{Q}, \mathcal{K}, \mathcal{V} \in \mathbb{R}^{L \times d}$ shares a hidden dimension d , with L being the number of total tokens. The attention module Attn is then formulated as $\text{Attn}(\mathcal{Q}, \mathcal{K}, \mathcal{V}) = \text{softmax}(\frac{\mathcal{Q}\mathcal{K}^T}{\sqrt{d}})\mathcal{V}$. To be specific, let $\mathcal{Q} = [q_1, q_2, \dots, q_L]$ and $a_i = \text{softmax}(\frac{q_i\mathcal{K}^T}{\sqrt{d}}) \in \mathbb{R}^L$ is the attention scores for the i th token p_i . As for the multi-head self-attention, \mathcal{H} self-attention modules are applied to $\{p_i\}_{i=1}^L$ separately, and a weighted averaging is then performed on top of their outputs to generate the final representation. The corresponding attention score is modified as $\tilde{a}_i = \frac{1}{\mathcal{H}} \sum_{h=1}^{\mathcal{H}} a_i^h$.

3.1 CancerMoE - An Ultra-Efficient Multi-Modal Integration Framework in Cancer Prognosis

Overview of CancerMoE. CancerMoE is a multi-modal integration algorithm that learns and infers from histology and genomics information for cancer prognosis. Together with a tailored SMOE architecture, two

efficient designs are proposed from data (*i.e.*, dynamic patch selection in Section 3.3) and model (*i.e.*, attention consolidation and sparsification in Section 3.4) perspectives, aiming for fast cancer prognosis. The overall procedures of **CancerMoE** are illustrated in Fig. 2. It first selects the most influential histological image patches in a data-driven manner. Then, it turns all raw modalities into embeddings and feeds them into a unified transformer encoder to fuse the knowledge across modalities. Finally, all token embeddings are passed through our customized SMOE equipped with consolidated and sparsified attention modules. After this step, these tokens are fed to corresponding experts via modality-specific routing for cancer prognosis prediction.

Customized SMOE Architecture. In this work, we focus on transformed-based networks since they have demonstrated numerous successes in unifying heterogeneous modalities Zhu et al. (2022a). Our tailored designs span two aspects: ① *Modality-Specific Embedding and Routing Policies*. **CancerMoE** creates modality-specific embedding by concatenating the one-hot modality index vector and the token embedding as $\mathbf{x}_m = \text{Concat}(\mathbf{x}, \text{OneHot}(m))$, where \mathbf{x} and $\text{OneHot}(m)$ denote the intermediate token embedding and its one-hot index vector of the modality m , respectively. On top of \mathbf{x}_m , modality-aware routing is enabled according to $\mathcal{R}(\mathbf{x}_m)$. The design philosophy is to encourage a synergized multi-modal optimization by learning appropriate modality-*specific* and -*agnostic* expert assignments, which provides possibilities to uncover hidden cross-modality interactions and transcends the capabilities of any single modality, as demonstrated in Sec. 4.4.

② *Modularization*. For efficiency purposes, we turn a large, densely connected model into the mixture-of-experts architecture. Specifically, a uniform partition is adopted to divide the original MLP into multiple smaller MLPs. Without loss of generality, let d be the dimensionality of the original MLP. After our modularization, a series of MLP experts $\{f_1, f_2, \dots, f_E\}$ is obtained with the same hidden dimension $\frac{d}{E}$. Note that, at both training and inference phases, only a small subset of experts are activated for the prediction of one sample, facilitating efficient cancer prognosis (Table 2). Meanwhile, such model division allows a disentanglement in the model parameter space, offering opportunities to mitigate conflicted gradient directions from diverse modalities (Figure 5 (b)).

3.2 Genomic Profile Encoder

To integrate genomic information, we use "PatchEmbedding" to encode the genomic profiles. Specifically, we start by treating the genomic profiles as a single vector, which we divide into g sub-vectors. Each sub-vector is then projected into the embedding space through a linear layer. After this, we concatenate the sequence of genomic profile tokens with the image tokens to create a single input sequence. This combined sequence is then processed by the transformer backbone, where the self-attention modules merge the two types of data.

3.3 Dynamic Patch Selection for Cancer Images with Super High Resolutions

The fine-gained histological image information is necessary for prognosis Shaban et al. (2019); Kim et al. (2020). Nevertheless, there are two challenges that hinder the effective and efficient utilization of this special modality for prognosis: (1) the super-high-resolution Whole Slide Images (WSIs) result in unbearable computation costs; (2) the interfering noise level increases with the image resolution.

To tackle these issues, we present the Dynamic Patch Selector (DPS) framework. The DPS begins by segmenting all whole slide images (WSIs) into patches and storing them in the patch bank for each example. Partial patches then undergo a dynamic scoring process, through which a small subset of the most informative patches, deemed worthy of learning, is selected. Simultaneously, a random subset of the remaining patches within the patch bank is also chosen to prevent overfitting and explore other informative patches. Subsequently, the chosen patches are collaboratively used for the online training of our proposed **CancerMoE** framework, resulting in significant training cost reductions and effective noise token filtration.

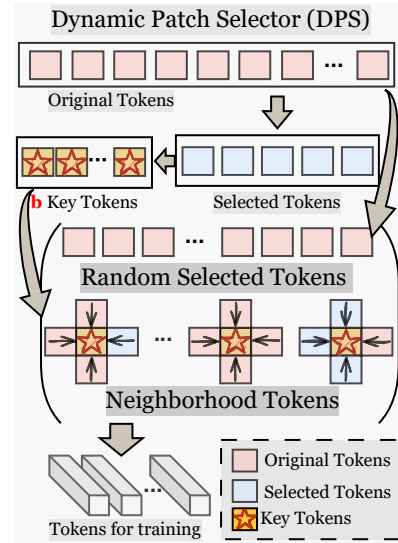


Figure 3: The procedure of Dynamic Patch Selector (DPS).

Proposed Remedies of Addressing the Redundancy Issues to Recover Efficiency. Recently, Rao et al. (2021); Kong et al. (2021) have observed the information contained in tokens has diverse ranges, which indicates that there are redundant and noisy tokens among the WSIs. We can remove less informative tokens to save computational costs and filter noisy tokens to achieve superior performance.

Our policy for managing computational costs involves reviewing a fixed number of WSI tokens during each training iteration. This subset comprises two distinct parts: neighborhood tokens and randomly selected tokens. As depicted in Figure 3, tokens processed by the network will be assigned a token score, hereafter referred to as “Selected Tokens”. The DPS first retrieves b tokens with the highest token scores, designated as “Key Tokens”, which treats them as informative tokens. Intuitively, informative tokens are not isolated, regions surrounding “Key Tokens” are likely to contain pertinent information. For instance, the extent of cancerous tissue often surpasses the size of a single patch (each patch will be processed as a token). Hence, we select tokens centered on “Key Tokens” as neighborhood tokens. However, in the initial stages of training, the token scores from the attention mechanism could be inaccurate, potentially leading to network overfitting on less informative tokens. To mitigate this, the DPS concurrently retrieves tokens from the “Original Tokens” at random- termed “Random Selected Tokens”. This parallel selection process explores new informative tokens and prevents overfitting to initially favored yet sub-optimal tokens.

Token score from self attention., for token score assignment, we introduce the unique learnable token, denoted as \mathbf{x}_{cls} . \mathbf{x}_{cls} will be inserted at the beginning of each input sequence to accumulate information from other tokens. We compute the token score from its attention score $a_{\text{cls}} = \text{softmax}(\frac{q_{\text{cls}}\mathcal{K}^T}{\sqrt{d}}) \in \mathbb{R}^L$, where q_{cls} is the query vector of \mathbf{x}_{cls} . **The attention score comes from the intrinsic attention mechanism in our transformer-based backbone do not require any additional cost.** Each element in a_{cls} corresponds to a token in the input sequence and is expressed as its associated token score.

Details of Dynamic Patch Selection Mechanism. We first split all WSIs of each example to construct a patch bank, then, as nailed in Fig. 3, we identify the neighborhood tokens during each item at first. We select b key tokens with Top- b attention scores, usually, the value of b is ding to 4. A more comprehensive discussion on the number of b key tokens can be found in Sec. 4.4, where additional details are provided.

We use ResNet to encode fixed-size image sub-regions, resulting in different image sizes producing varying numbers of tokens. For example, for SKCM, the average number of tokens is 58,381, the maximum is 1,010,257, and the minimum is 923. This variation in the number of tokens makes parallel training challenging, as it requires input data to have the same shape to form a batch for network training. CancerMoE addresses this issue by fixing the number of tokens for each input WSI to (N) , enabling parallel training. Then extract $N \times (1 - p)$ tokens around these b tokens as part of selected tokens for DPS, where p is the ratio of selected unseen tokens. For the remaining $N \times p$ tokens of DPS, we uniformly select them among the unused original tokens to explore more informative tokens and avoid overfitting to neighborhood tokens. However, the weight of the model is continuously updated during the training epoch, which actively keeps changing the attention value of the same token. Hence, for a stable output, we update the token score only when the c-index of the training set decreases. For more details about the token score update method and DPS please refer to Section 4.4.

3.4 Attention Consolidation and Sparsification

Algorithm 1 Attention Sparsification, $\mathcal{A}_i(\mathbf{x})$

Require: query, key, and value of \mathbf{x} $\mathcal{Q}, \mathcal{K}, \mathcal{V}$

- 1: $\mathcal{A} = \text{softmax}(\frac{\mathcal{Q}\mathcal{K}^T}{\sqrt{d}})$ # Calculate the attention map
- 2: Calculate $k \leftarrow (q \times N)^2$, $\mathcal{A}_{\text{flat}} \leftarrow \text{Flatten}(\mathcal{A})$
- 3: $\mathcal{A}_{\text{top}} \leftarrow \text{TopK}(\mathcal{A}_{\text{flat}}, k)$, $\mathcal{A}_{\text{sparse}} \leftarrow \text{Reshape}(\mathcal{A}_{\text{top}})$
- 4: **return** $\mathcal{A}_{\text{sparse}}\mathcal{V}$

Owing to the redundancy among attention heads Michel et al. (2019); Beltagy et al. (2020), it motivates us to consolidate learned information, which can enable efficient prediction of cancer patient’s survival rates.

Algorithm 2 Attention Consolidation**Require:** Attention importance scores: $\{I_1, I_2, \dots, I_{\mathcal{H}}\}$ **Ensure:** Attention Head output: $\{\mathcal{A}_1(\mathbf{x}), \mathcal{A}_2(\mathbf{x}), \mathcal{A}_{\mathcal{H}}(\mathbf{x})\}$

```

1:  $\{\mathcal{A}_1^{(1)}, \mathcal{A}_1^{(2)}, \dots, \mathcal{A}_1^{(k)}\} = \text{Topk}(\{I_1, I_2, \dots, I_{\mathcal{H}}\}, \{\mathcal{A}_1(\mathbf{x}), \mathcal{A}_2(\mathbf{x}), \mathcal{A}_{\mathcal{H}}(\mathbf{x})\})$  # Use importance scores to
   select important heads
2:  $\mathbf{y} = \{\}$  # Attention output
3: for  $\mathcal{A}_1^{(i)}$  in  $\{\mathcal{A}_1^{(1)}, \mathcal{A}_1^{(2)}, \dots, \mathcal{A}_1^{(k)}\}$  do
4:    $\mathcal{A}_{cluster}^{(i)} = \{\}$  # Attention Cluster
5:    $\mathcal{I}_{cluster}^{(i)} = \{\}$  # Attention importance score in the cluster
6:   for  $\mathcal{A}_j(\mathbf{x})$  in  $\{\mathcal{A}_1(\mathbf{x}), \mathcal{A}_2(\mathbf{x}), \mathcal{A}_{\mathcal{H}}(\mathbf{x})\}$  do
7:     if  $\text{COSINE}(\mathcal{A}_1^{(i)}(\mathbf{x}), \mathcal{A}_j(\mathbf{x})) \leq \{\text{COSINE}(\mathcal{A}_1^{(t)}(\mathbf{x}), \mathcal{A}_j(\mathbf{x}))\}_{t \neq i, t=1}^{t=k}$  then
8:       Add  $\mathcal{A}_j$  to  $\mathcal{A}_{cluster}^{(i)}$ 
9:       Add  $\mathcal{I}_j$  to  $\mathcal{I}_{cluster}^{(i)}$ 
10:    end if
11:  end for
12:   $y_i \leftarrow \mathbf{0}$ 
13:  for  $A_i$  in  $\mathcal{A}_{cluster}^{(i)}$  do
14:     $y_i = y_i + \text{softmax}(\mathcal{I}_{cluster}^{(i)})_i \times \mathcal{A}_i(\mathbf{x})$ 
15:  end for
16:  Add  $y_i$  to  $\mathbf{y}$ 
17: end for

```

Our attention consolidation and sparsification (ACS) algorithm consists of two components: (1) *attention consolidation*, where attention maps are clustered based on their cosine similarity and then merged into a few more knowledge ones; (2) *attention sparsification*, where superfluous attention connections are trimmed for extra inference efficiency.

▷ *Attention Consolidation.* As shown in Fig. 2 and Algorithm 2, we first calculate the importance score $\{I_1, I_2, \dots, I_{\mathcal{H}}\}$ of all attention heads $\{\mathcal{A}_i\}_{i=1}^{\mathcal{H}}$ to identify the most informative ones, where \mathcal{H} is the number of attention heads. To be specific, the importance of attention head \mathcal{A}_i is estimated as:

$$I_i = \mathbb{E}_{\mathbf{x} \sim \mathcal{X}} \left| \mathcal{A}_i(\mathbf{x})^\top \frac{\partial \mathcal{L}(\mathbf{x})}{\partial \mathcal{A}_i(\mathbf{x})} \right|, \quad (2)$$

where \mathcal{X} symbolizes the distribution of training data, $\mathcal{L}(\mathbf{x})$ signifies the objective function, and $\mathcal{A}_i(\mathbf{x})$ represents the output features.

Then, k informative attention heads are selected, and K-means is applied to assign the rest of the attention heads to these k informative ones, according to their cosine similarities. In this way, $\{\mathcal{A}_1^{(1)}, \mathcal{A}_1^{(2)}, \dots, \mathcal{A}_1^{(k)}\}$ denotes the k selected attention heads. Their associated sets of clustered heads are $\{\{\mathcal{A}_2^{(1)}, \dots, \mathcal{A}_{n_1}^{(1)}\}, \{\mathcal{A}_2^{(2)}, \dots, \mathcal{A}_{n_2}^{(2)}\}, \dots, \{\mathcal{A}_2^{(k)}, \dots, \mathcal{A}_{n_k}^{(k)}\}\}$, where $\{n_1 - 1, \dots, n_k - 1\}$ are the number of allocated heads and $\sum_{i=1}^k n_i = \mathcal{H}$. The output \mathbf{y}_i from the cluster i is described as a weighted sum across n_i heads:

$$\mathbf{y}_i = \underbrace{\text{softmax}(\{I_1, \dots, I_{n_i}\})_i}_{\text{The } i\text{th informative attention head}} \times \mathcal{A}_i(\mathbf{x}) + \sum_{j=2}^{n_i} \underbrace{\text{softmax}(\{I_1, \dots, I_{n_i}\})_j}_{\text{Allocated attention heads in the cluster } i} \times \mathcal{A}_j(\mathbf{x}). \quad (3)$$

The final output from the consolidated multi-head attention can be formulated as $\mathbf{y} = \text{Concat}(\{\mathbf{y}_i\}_{i=1}^k)$.

▷ *Attention Sparsification.* In Fig. 2 and Algorithm 1, to remove superfluous attention connections, we further sparsify attention maps by only preserving $(q \times N)^2$ attention elements with the largest magnitude. q is a pre-defined ratio for the attention sparsification and N represents the number of WSIs' tokens. Note that,

Table 1: Performance comparison of our model vs. diverse baselines on 12 cancer diagnostic datasets. The notation ‘‘P.’’ signifies the utilization of pathological images, ‘‘G.’’ indicates the use of genomic profiles, and ‘‘M.’’ implies the incorporation of both pathological images and genomic profiles. We mark the best performance in **bold** and the second best performance in underline.

Method	Modality	BLCA	BRCA	HNSC	KIRC	KIRP	LIHC	LUAD	LUSC	PAAD	SKCM	STAD	UCEC	Overall \uparrow
SNN(NeurIPS'17) Klambauer et al. (2017)	G.	<u>0.632</u>	0.573	0.577	0.665	0.707	0.570	0.591	0.522	0.537	0.519	0.545	0.601	0.596
OmicMIP(Preprint'23) Jaume et al. (2023)	G.	0.581	0.589	0.542	0.658	0.740	0.541	0.582	0.507	0.578	0.590	0.527	0.604	0.587
AttnMISL(ICML'18) Ilse et al. (2018)	P.	0.553	0.561	0.543	0.577	0.622	0.629	0.564	0.555	0.538	0.621	0.559	0.617	0.581
DeepAttnMISL(MIA'20) Yao et al. (2020)	P.	0.596	0.681	0.569	0.508	0.698	0.625	0.647	0.558	0.594	0.632	0.567	0.743	0.618
Patch-GCN(MICCAI'21) Chen et al. (2021a)	P.	0.560	0.580	0.562	0.524	0.644	<u>0.671</u>	0.585	<u>0.571</u>	0.585	<u>0.666</u>	0.541	0.629	0.611
TransMLL(NeurIPS'21) Shao et al. (2021)	P.	0.529	0.524	<u>0.602</u>	0.533	0.605	0.650	0.476	0.498	0.538	0.637	0.523	0.538	0.554
MCAT(ICCV'21) Chen et al. (2021b)	M.	0.624	0.580	0.557	0.661	0.771	0.636	0.620	0.503	<u>0.627</u>	0.613	0.514	0.622	0.610
CLAM-SB(Nat. Biomed. Eng.'21) Lu et al. (2021)	P.	0.549	0.598	0.577	0.573	0.610	0.645	0.566	0.545	0.541	0.629	0.562	0.599	0.583
CLAM-MB(Nat. Biomed. Eng.'21) Lu et al. (2021)	P.	0.553	0.585	0.541	0.567	0.623	0.630	0.565	0.561	0.554	0.626	0.566	0.581	0.579
PorpoiseAMIL(Cancer Cell'22) Chen et al. (2022b)	P.	0.542	0.560	0.564	0.567	0.539	0.618	0.548	0.561	0.580	0.607	0.556	0.638	0.584
MMF(Cancer Cell'22) Chen et al. (2022b)	M.	0.627	0.558	0.580	<u>0.711</u>	<u>0.811</u>	0.640	0.586	0.527	0.391	0.608	0.587	0.644	<u>0.629</u>
Surformer(CMPB'23) Wang et al. (2023)	P	0.553	<u>0.623</u>	0.576	0.520	0.594	0.678	0.580	0.549	0.544	0.640	0.606	0.592	0.588
CMTA(ICCV'23) Zhou & Chen (2023)	M	0.619	0.613	0.587	0.617	0.802	0.567	0.642	0.646	0.556	0.590	0.556	0.590	0.616
Ours	M.	0.653	0.576	0.603	0.752	0.824	0.647	<u>0.644</u>	<u>0.571</u>	0.634	0.687	<u>0.605</u>	<u>0.660</u>	0.655

at the inference phase, the attention calculation purely happens among the selected $q \times N$ tokens, leading to substantially reduced computational costs. Finally, these consolidated and sparsified tokens are processed by task-specific heads to determine the cancer prognosis.

3.5 Multi-modal Fusion for Dynamic Patch Selection

With the DPS and ACS, we have achieved substantial training efficiency. Nonetheless, the performance remains suboptimal. We hypothesize that the limitation arises from the inadequacy of token selection by the DPS. To address this issue, integrating additional modalities is proposed to further enhance the DPS and then achieve more competitive performance. We pack adjacent genes into tokens to construct the genomic sequence as an additional modality. In our **CancerMoE** framework, we consolidate all modalities pertaining to a single input into a unified sequence. This is achieved by leveraging the self-attention mechanism to fuse cross-modal information. This design strategy not only facilitates the seamless integration of multi-modal data without necessitating structural modifications but also promotes the DPS by effectively utilizing other modal information. The benefits and advancements of our design are further elaborated in Table 3.

4 Experiment

4.1 Implementation Details.

Datasets. To evaluate our proposed **CancerMoE**, we conduct experiments on The Cancer Genome Atlas (TCGA), a publicly accessible database housing genomic and clinical data derived from thousands of cancer patients, encompassing 33 prevalent cancer types. The Cancer Genome Atlas (TCGA) is a publicly accessible database housing genomic and clinical data from thousands of cancer patients, encompassing 33 prevalent cancer types commonly used in cancer prognosis prediction. We select 12 cancer types that are frequently used in plenty of works Chen et al. (2021c); Klambauer et al. (2017); Jaume et al. (2023); Ilse et al. (2018); Chen et al. (2021a); Shao et al. (2021; 2023); Chen et al. (2021b); Lu et al. (2021); Chen et al. (2022b). We utilize the pre-processed Whole Slide Image (WSI) is proposed by Chen et al. (2022b) as the image input for **CancerMoE**. The WSI is segmented 256×256 sub-images of high-resolution histology images and extracts each sub-image into feature vector \mathbb{R}^{1024} by CLAM Lu et al. (2021). The size of the different WSIs varies greatly ($8, 417 \times 6, 602$ to $191, 352 \times 91, 562$), resulting in the number of paths \mathbb{R}^{1024} also varies accordingly, which makes parallelizing the training process difficult. More details about datasets and implementation can be found in Appendix A.

Optimization Object. To optimize the model parameters, we utilize the log-likelihood function for a discrete survival model Chen et al. (2022b), L_c , where L_c is the loss function for the censor patients. Formally, the survival state of a patient considers two factors: 1) Censorship status, where $c = 0$ signifies an observed patient death and $c = 1$ corresponds to the patient’s last known follow-up. 2) Time-to-event, represented as t_i , signifies the duration between the patient’s diagnosis and observed death if $c = 0$, or the time until the

last follow-up if $c = 1$. The h denotes the output representing discrete survival predictions:

$$\text{hazards} = \sigma(h). \quad (4)$$

In the next step, the cumulative survival function $S(t)$ is calculated from the hazards:

$$S(t) = \prod_{i=0}^t (1 - \text{hazards}_i). \quad (5)$$

Then the final loss function \mathcal{L}_c corresponding to censored patients is defined as:

$$\mathcal{L}_c = -(1 - c) \cdot (\log(\mathcal{S}(t - 1)) + \log(\mathcal{S}(t))). \quad (6)$$

The term of the loss function corresponding to uncensored patients \mathcal{L}_u is defined as:

$$\mathcal{L}_u = -c \cdot \log(\mathcal{S}(t)). \quad (7)$$

The final loss function can be obtained by combining \mathcal{L}_c and \mathcal{L}_u . The β is the hyperparameter that balances the two loss terms.

$$\mathcal{L}_{\text{survival}} = (1 - \beta) \cdot \mathcal{L}_c + \beta \cdot \mathcal{L}_u \quad (8)$$

Evaluation Metric. The performance of the models is assessed using the concordance index (c-index) Harrell et al. (1982), where higher values indicate better performance. The c-index measures the proportion of all possible pairs of observations for which the model’s predicted values accurately predict the ordering of actual survival. It ranges from 0.5 (indicating random prediction) to 1 (reflecting perfect prediction). The c-index can be expressed with the following formulation:

$$\text{c-index} = \frac{1}{n(n-1)} \sum_{i=1}^n \sum_{j=1}^n I(T_i < T_j)(1 - c_j), \quad (9)$$

where n is the sample size, T_i and T_j represents the survival time of the i -th and j -th patients. The symbol $I(\cdot)$ denotes the indicator function, which evaluates to 1 if its argument is true and 0 otherwise. Meanwhile, c_j indicates the correct censorship status.

We follow the evaluation of Chen et al. (2021c); Klambauer et al. (2017); Jaume et al. (2023); Ilse et al. (2018), which utilize 5-fold cross-validation to demonstrate the superiority of our method.

Model Implementation Details. SMoE: We employ two transformer encoder layers, and the SMoE is tailored in the MLP layer of the last transformer encoder layers. The number of experts is 4 or 8, and we use the load and importance balancing loss Shazeer et al. (2017b) to combat the imbalance loading phenomenon Chi et al. (2022). DPS: We use the attention score of the last transformer encoder layers as the token scores. For the neighborhood tokens, assuming the number of neighborhood regions is N_n , the total number of tokens is N , and the ratio of select unseen tokens is p . We will select $N \times (1 - p)/(2N_n)$ tokens on the right and left sides of the Key Token, respectively. ACS: We do consolidation on each transformer encoder layer. The sparsification is only executed in the first transformer encoder layer, where we filter 92% WSIs tokens. Model Architecture: The number of attention heads is 8, the hidden dimension of our model is 32. For the genomic profiles, we use a patch embedding layer that splits each gene profile vector into sequences with length 8. Training: The training batch size is set to 32, and the learning rate is $1e^{-3}$. **For other important hyperparameters, we use the same default settings for all cancer types except BRCA, LUSC, and SKCM: 3072 selected tokens, 4 key tokens, and a ratio of 0.5 for selecting unseen tokens.**

4.2 Powerful performance of CancerMoE in fierce competitions

In this section, we fairly compare the performance of our model with various state-of-the-art baselines. The involved machine learning models are SNN Klambauer et al. (2017), OmicMIP Jaume et al. (2023), AttnMISL Ilse et al. (2018), Patch-GCN Chen et al. (2021a), TransMIL Shao et al. (2021), MCAT Chen

Table 2: Parameters, FLOPs, VRAM consumption, and Training time of **CancerMoE** *v.s.* diverse baselines that involve pathological images. The VRAM consumption of each method is in the training stage (Average VRAM consumption across all cancer datasets), and the training time is the average time for all 12 cancers. We mark the best performance in **bold** and the second in underline.

Method	Modality	Params(M)↓	FLOPs(G)↓	VRAM(G)↓	Training time(H)↓
AttnMISL Ilse et al. (2018)	P.	0.920	42.189	7.320	4.861
Patch-GCN Chen et al. (2021a)	P.	1.187	<u>2.545</u>	20.843	4.974
TransMIL Shao et al. (2021)	P.	0.275	11.743	12.117	8.001
MCAT Chen et al. (2021b)	M.	3.210	7.823	<u>6.003</u>	6.479
CLAM-SB Lu et al. (2021)	P.	0.790	14.707	7.007	<u>4.327</u>
CLAM-MB Lu et al. (2021)	P.	0.791	39.842	8.053	6.317
PorpoiseAMIL Chen et al. (2022b)	P.	0.937	40.872	13.294	5.747
DeepAttnMISL Yao et al. (2020)	P.	8.532	33.294	4.417	12.047
Surformer Wang et al. (2023)	P.	14.520	18.534	4.898	4.343
MMF Chen et al. (2022b)	M.	6.849	137.24	12.376	7.324
Ours	M.	<u>0.446</u>	0.170	1.875	2.362

et al. (2021b) and **CMTA(ICC’23) Zhou & Chen (2023)**, and biology literature-based methods include CLAM-SB Lu et al. (2021), CLAM-MBLu et al. (2021), MMF Chen et al. (2022b), PorpoiseAMIL Chen et al. (2022b), and Surformer Wang et al. (2023). Given that single-modal approaches still exhibit superior performance for certain cancers, we also compare our model with single-modal baselines that utilize either only pathological images or genomic profiles. The whole comparison results of **CancerMoE** *v.s.* baselines on 12 type of cancers are shown in Table 1, in which we make the following three observations. ① **CancerMoE** achieves the highest overall performance across all 12 cancer datasets. Specifically, **CancerMoE** exceeds biology-based and learning-based baselines {0.026, 0.071, 0.068}, and {0.094, 0.072, 0.062} in cancers {KIRC, BLCA, LUAD}, respectively. These empirical results demonstrate the effectiveness of our model in addressing the cross-modality conflict and assigning plausible SMOE experts to conduct better cancer prognosis prediction. ② On LIHC and BRCA, the performance of **CancerMoE** merely achieves a moderate level. The best performance of these two cancer types is achieved by methods Patch-GCN Chen et al. (2021a) and CLAM-SB Lu et al. (2021) that only use WSI images, which indicates **we need a more comprehensive fusion mechanism to effectively integrate genomic profiling with histological image in LIHC and BRCA**. ③ Our multimodal approach outshines competing baselines in resolving modality conflicts across diverse cancer datasets, evident in consistently superior performance metrics in the c-index. By seamlessly integrating information from pathological images and genomic profiles, our model excels in {KIRC, BLCA, LUAD SKCM}, surpassing MMF Chen et al. (2022b) {0.041, 0.021, 0.024, 0.021}, beating MCAT Chen et al. (2021b) {0.091, 0.029, 0.024, 0.074}. These results prove our model’s efficacy in leveraging complementary modalities, effectively addressing and reconciling conflicts for enhanced cancer diagnostic accuracy.

4.3 Superior Efficiency Across Diverse Baselines.

Given the extremely high dimensionality of image data in pan-cancer diagnosis, we investigate the efficiency of **CancerMoE** compared to baseline models. In Table 2, we advance deeply to demonstrate the advance of **CancerMoE** on efficient training and inference. **CancerMoE** achieve improved performance with much fewer computational resources in terms of fewer data patches and training epochs. The flops of **CancerMoE** is solely **1/1000** of that of MMF Chen et al. (2022b), yet manifests a considerable qualitative improvement. Compared to MCAT Chen et al. (2021b), **CancerMoE** use 1/50 computation complexity, with a 7.4% higher c-index, which clearly shows the superiority and viability of our method. What is even more noteworthy is that with the same granularity choices including batch and patch size, **CancerMoE** only utilizes 9%-20% GPU memory (VRAM) of previous methods. Moreover, in a direct comparison with baselines, **CancerMoE** consistently outperforms in the competition.

4.4 Ablation and Additional Investigations.

Ablation on each component in CancerMoE. To validate the effectiveness of each component in **CancerMoE**, we conduct ablation studies as recorded in Table 3. Results indicate that (1) **ACS** is the central performance contributor; (2) The designs of **DPS** and **SMoE** bring similar level amounts of performance improvements; (3) The combination of above three leads to a superior result in cancer prognosis; (4) The superior performance compared with “*w/o DPS*” that selects tokens randomly, demonstrate the efficacy of **DPS** in finding important tokens. (5) In the **LUSC** dataset, employing genomic profiles without the **SMoE** framework yields inferior results compared to using only **WSIs** (“*w/o SMoE*” versus “*w/o Genomic Profiles*”), which suggests the presence of gradient conflicts, in which **SMoE** effectively mitigates. (6) The enhancement in performance when moving from “*w/o Genomic Profiles*” and “*w/o DPS*” to the **CancerMoE** model demonstrates the benefit of incorporating additional modalities. It leads to selecting elite tokens better by **DPS** and leverages genomics data to promote prediction accuracy.

Table 3: Ablation studies on **DPS**, **ACS**, **SMoE**, and fusion. We fix a set of randomly selected tokens during training to replace the **DPS** as “*w/o DPS*”, use the vanilla attention module to replace the **ACS** as “*w/o ACS*”, use the dense MLP module with the same parameter to replace the **SMoE** layer as “*w/o SMoE*”, and remove genomic profiles as “*w/o Genomic Profiles*”. The “**Random Select**” replaces the **DPS** policy with policy that keep random token selection during training and inference.

Setting	BRCA	LUSC	SKCM
CancerMoE	0.576	0.571	0.687
- <i>w/o DPS</i>	0.564	0.519	0.655
- <i>w/o ACS</i>	0.541	0.506	0.641
- <i>w/o SMoE</i>	0.565	0.493	0.665
- <i>w/o Genomic Profiles</i>	0.539	0.525	0.515
- Random Select	0.555	0.529	0.567

Table 4: Ablation on # selected tokens (N) of **CancerMoE**.

N	BRCA	LUSC	SKCM
512	0.569	0.571	0.654
1024	0.576	0.547	0.651
2048	0.566	0.536	0.655
3072	0.515	0.509	0.687
4096	0.546	0.536	0.643

Table 5: Ablation studies on # Key Tokens (b) of **CancerMoE**.

Setting	BRCA	LUSC	SKCM
1	0.570	0.548	0.626
2	0.573	0.527	0.636
3	0.570	0.559	0.627
4	0.571	0.571	0.687
5	0.576	0.567	0.642

Table 6: Ablation on # informative attention heads in **ACS**.

Setting	BRCA	LUSC	SKCM
0.1	0.537	0.555	0.600
0.3	0.561	0.544	0.687
0.5	0.576	0.571	0.666
0.7	0.572	0.527	0.624
0.9	0.571	0.565	0.655

DPS - The Number of Selected Tokens. The results in Table 4 show that ① The best number of selected tokens is dataset-dependent. Results vary from dataset to dataset. We present clear indications on **BRCA**, **LUSC**, and **SKCM** datasets. For **BRCA**, the performance pinnacle is reached at $N = 1024$, with **LUSC** and **SKCM** arriving at a sweet point for superior predictions at N values of 512 and 3072, correspondingly. ② The performance shows an upward trend as the value of N increases. This observation highlights that too small a number of tokens do not provide enough feature information for the **DPS** to capture. ③ Following its peak, we obviously note that the performance experiences a gradual decline as N values increase, which indicates that abundant tokens do not necessarily yield superior outcomes. Although **DPS** selects quality patches for training, more tokens inevitably introduce noise, affecting performance.

Table 7: Ablation studies on different token score update policies of our proposed **CancerMoE**. “per epoch” denotes the update token score every epoch, “ n epoch apart” denotes the update token score n epoch apart, and “ c -index depends” denotes token score is updated when the c -index of the training set decrease.

Setting	BRCA	LUSC	SKCM
per epoch	0.570	0.528	0.656
1 epoch apart	0.560	0.520	0.662
2 epochs apart	0.564	0.523	0.652
4 epochs apart	0.562	0.521	0.664
c -index depends	0.576	0.571	0.687

DPS - The Number of Key Tokens b . The ablation experiments on the number of Key Tokens b are presented in Table 5, it is verified on datasets **BRCA**, **LUSC**, and **SKCM**. The optimal diagnostic benefit is achieved when the value of b is set to 4, too small or too large of b , both causing performance degradation. The finding shows the importance of the number of neighborhood tokens, which is crucial to identifying diagnostic information.

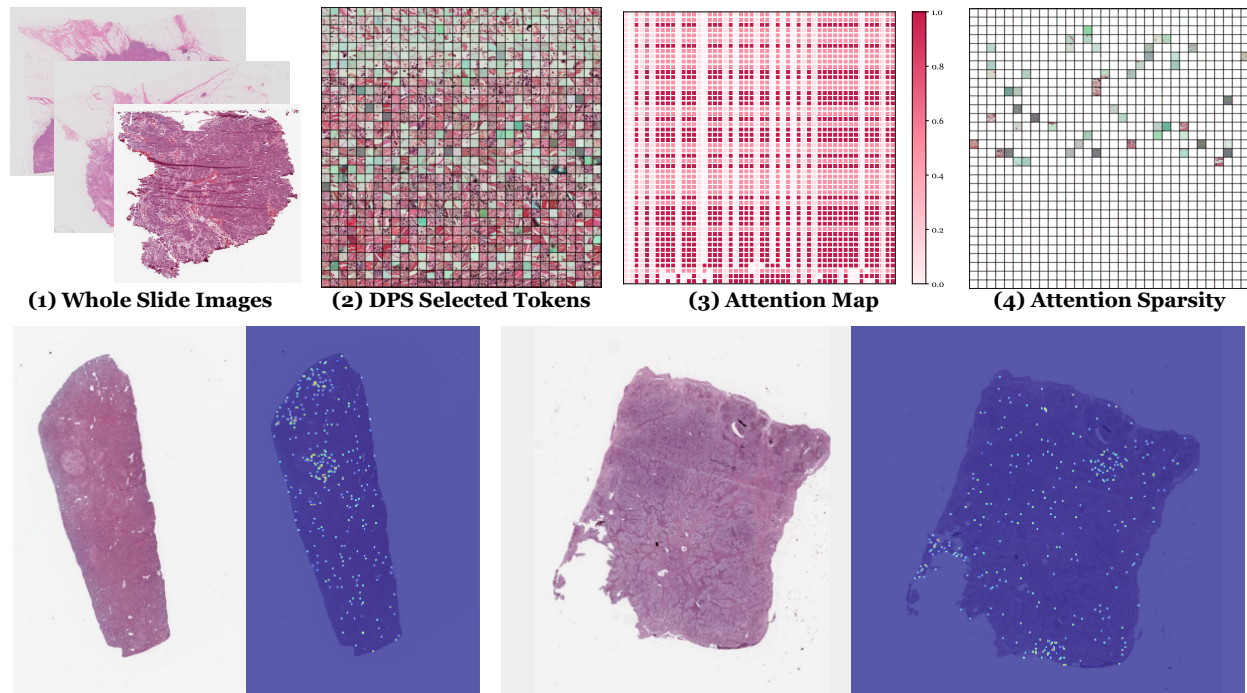


Figure 4: **Top:** Analysis of the diversified attention via attention sparsity. These blocks are selected tokens for critical region identification, and colorful blocks are unmasked attention tokens. **Bottom:** Additional visualized attention scores identified by CancerMoE.

DPS - Token Score Update Policy. As shown in Table 7, adopting different token score update policies influences the performance of CancerMoE. On the BRCA, SKCM cancer dataset, the “c-index depends” approach exhibits superior predictive capabilities, outperforming the “4 epochs apart” and “2 epochs apart” strategies. Moreover, the “c-index depends” tactics demonstrate more impressive competitiveness on the LUSC dataset. Compared with the sub-optimal one, the “c-index depends” exceeds 0.043. Considered holistically, we determine that “c-index depends” represents the most effective token score update policy.

DPS - The Ratio p of Select Unseen Tokens. The ratio p of select unseen tokens indicates how much the overview information we use for prognosis prediction. We also conducted extensive investigations on the ratio p illustrated in Table 6. Initially, as the ratio increased, the accuracy of prognostic diagnosis improved. Subsequently, the optimal performance plateaued at $p = 0.5$, reaching a saturation state. Increasing the parameter p allows the model to encounter a broader range of new tokens, thereby mitigating the risk of overfitting to a limited set of specific tokens. However, setting p too high can be counterproductive, as it may lead the model to sample tokens too randomly, which can obstruct the model’s ability to converge effectively. The observation highlights that the balance between local and overview WSI information is critical and needs to be carefully determined.

ACS - Consolidation and Sparsification In order to substantiate our proposition that eliminating redundant information carried by redundant attention heads can result in remarkable advancements in cancer prognostic performance, we performed fusion experiments by varying the diverse number of attention heads, and the resultant findings are presented in Table 8. The data reveals that aggregating multiple heads brings substantial advantages without any accompanying disadvantages. Notably, the most gratifying outcomes are obtained when 2 is chosen as the number of informative attention heads.

Table 8: Ablation studies on the ratio p of selected unseen tokens of our proposed CancerMoE.

Setting	BRCA	LUSC	SKCM
<i>w/o Consolidation</i>	0.536	0.541	0.685
1	0.540	0.511	0.682
2	0.576	0.514	0.687
3	0.567	0.571	0.671

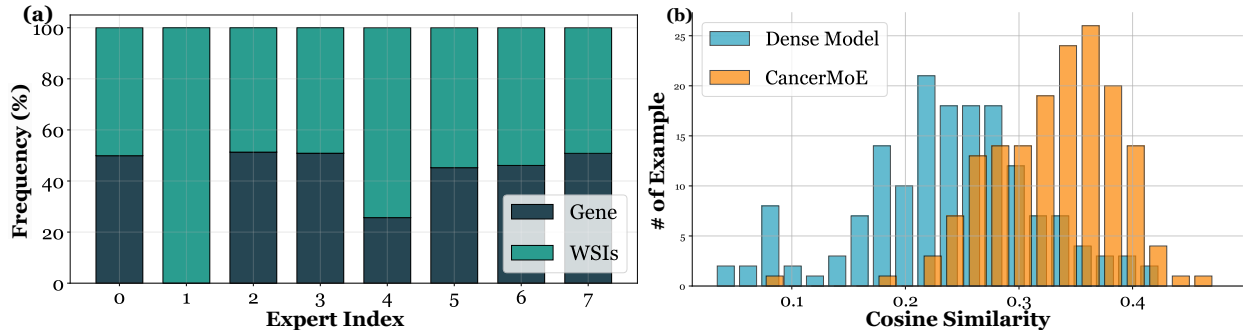


Figure 5: (a) The expert selection across different modalities in the BRCA dataset. (b) The gradient conflict between modalities in **CancerMoE** and the dense counterpart. Here, the gradients are obtained from the experts and dense MLP with the same configuration in **CancerMoE** and **Dense Model**, respectively. our proposed sparse model demonstrates reduced conflict, as evidenced by more positive cosine distances, thereby facilitating enhanced multi-modal integration. The BRCA dataset is used for the experiment. The gradient is collected from the last transformer layer. More positive cosine distances denote less gradient conflict.

ACS - Interpretability from Diversified Attention. To raise the interpretability of the model, we conducted experiments with a sparse algorithm for the self-attention module. The outcomes of the sparsity operation are displayed in Fig. 4, where we eliminate elements with low information content in the sequence to reduce inherent redundancy and improve efficiency.

SMoE - Modality Level Routing Specialization. To showcase the effectiveness of the modality router structure, we present a visualization of **CancerMoE** in Fig. 5 (a). It can be observed that the expert 1 and the expert 4, who ponder to be attributed to genomic profiles and others, tend to process both modalities.

Gradient Conflict between Modalities. As previously mentioned, our modality-specific routing policy directs modality embeddings towards compatibility experts, which in turn produce high-quality modality features. This strategy effectively addresses various modalities and segregates the network parameter space according to different modalities and tasks. As demonstrated in Fig. 5 (b), disentangling the model’s parameter space significantly reduces gradient conflict between modalities. This separation leads to enhanced performance, which is further demonstrated in Table 3.

5 Conclusion and Limitation

This paper proposes **CancerMoE**, a multi-modal cancer prognosis prediction pipeline, to address the high computing costs incurred by WSIs and the gradient conflict arising from the heterogeneity between histological and genomic data. Firstly, in **CancerMoE**, the Dynamic Patch Selection (DPS) module tackles the complexity of ultra-high resolution by only feeding elite patches. Then, the Sparse Mixture-of-Experts (SMoE) is tailored to disentangle model parameter space to mitigate the gradient conflict. Finally, the Attention Consolidation and Sparsification (ACS) mechanism is investigated to diminish attention redundancy and enhance the efficiency of training and inference steps. Our **CancerMoE** has demonstrated superior performance on cancer prognosis prediction, with the c-index significantly increasing in 12 types of cancer and beating all other methods. Moreover, the experiments indicate that **CancerMoE** is more efficient than SoTA methods in terms of FLOPs, VRAM, and training time. Our approach offers valuable insights and techniques for multimodal AI to aid in efficient cancer prognosis. This fosters interdisciplinary progress across biology, medicine, and computer science. As medical AI rapidly evolves, using multimodal AI in cancer prognosis is becoming a practical reality.

CancerMoE has exhibited its effectiveness and exceptional performance in cancer prognosis tasks through experiments on multiple cancer datasets; nevertheless, apart from histopathology images and genomics, there exist multiple other modalities, such as EHR (Electronic Health Records). Our future vision entails the establishment of a multi-cancer types medical diagnostic service, incorporating these diverse modalities

to enhance the capabilities of our proposed approach. The integration of additional modalities into our framework poses an intriguing question that necessitates further exploration.

References

- Alhabib Abbas and Yiannis Andreopoulos. Biased mixtures of experts: Enabling computer vision inference under data transfer limitations. *IEEE Transactions on Image Processing*, 29:7656–7667, 2020.
- Parnian Afshar, Farnoosh Naderkhani, Anastasia Oikonomou, Moezedin Javad Rafiee, Arash Mohammadi, and Konstantinos N Plataniotis. Mixcaps: A capsule network-based mixture of experts for lung nodule malignancy prediction. *Pattern Recognition*, 116:107942, 2021.
- Karim Ahmed, Mohammad Haris Baig, and Lorenzo Torresani. Network of experts for large-scale image categorization. In *Computer Vision–ECCV 2016: 14th European Conference, Amsterdam, The Netherlands, October 11–14, 2016, Proceedings, Part VII 14*, pp. 516–532. Springer, 2016.
- Zeyuan Allen-Zhu and Yuanzhi Li. What can resnet learn efficiently, going beyond kernels? *Advances in Neural Information Processing Systems*, 32, 2019.
- Raquel Aoki, Frederick Tung, and Gabriel L. Oliveira. Heterogeneous multi-task learning with expert diversity. *CoRR*, abs/2106.10595, 2021. URL <https://arxiv.org/abs/2106.10595>.
- Tadas Baltrušaitis, Chaitanya Ahuja, and Louis-Philippe Morency. Multimodal machine learning: A survey and taxonomy. *IEEE transactions on pattern analysis and machine intelligence*, 41(2):423–443, 2018.
- Khaled Bayoudh, Raja Knani, Fayçal Hamdaoui, and Abdellatif Mtibaa. A survey on deep multimodal learning for computer vision: advances, trends, applications, and datasets. *The Visual Computer*, pp. 1–32, 2021.
- Iz Beltagy, Matthew E Peters, and Arman Cohan. Longformer: The long-document transformer. *arXiv preprint arXiv:2004.05150*, 2020.
- Nathaniel Braman, Jacob WH Gordon, Emery T Goossens, Caleb Willis, Martin C Stumpe, and Jagadish Venkataraman. Deep orthogonal fusion: multimodal prognostic biomarker discovery integrating radiology, pathology, genomic, and clinical data. In *Medical Image Computing and Computer Assisted Intervention–MICCAI 2021: 24th International Conference, Strasbourg, France, September 27–October 1, 2021, Proceedings, Part V 24*, pp. 667–677. Springer, 2021.
- Ethan Cerami, Jianjiong Gao, Ugur Dogrusoz, Benjamin E Gross, Selcuk Onur Sumer, Bülent Arman Aksoy, Anders Jacobsen, Caitlin J Byrne, Michael L Heuer, Erik Larsson, et al. The cbio cancer genomics portal: an open platform for exploring multidimensional cancer genomics data. *Cancer discovery*, 2(5):401–404, 2012.
- Anika Cheerla and Olivier Gevaert. Deep learning with multimodal representation for pancancer prognosis prediction. *Bioinformatics*, 35(14):i446–i454, 2019.
- Richard J Chen, Ming Y Lu, Jingwen Wang, Drew FK Williamson, Scott J Rodig, Neal I Lindeman, and Faisal Mahmood. Pathomic fusion: an integrated framework for fusing histopathology and genomic features for cancer diagnosis and prognosis. *IEEE Transactions on Medical Imaging*, 41(4):757–770, 2020.
- Richard J Chen, Ming Y Lu, Muhammad Shaban, Chengkuan Chen, Tiffany Y Chen, Drew FK Williamson, and Faisal Mahmood. Whole slide images are 2d point clouds: Context-aware survival prediction using patch-based graph convolutional networks. In *Medical Image Computing and Computer Assisted Intervention–MICCAI 2021: 24th International Conference, Strasbourg, France, September 27–October 1, 2021, Proceedings, Part VIII 24*, pp. 339–349. Springer, 2021a.
- Richard J Chen, Ming Y Lu, Wei-Hung Weng, Tiffany Y Chen, Drew FK Williamson, Trevor Manz, Maha Shady, and Faisal Mahmood. Multimodal co-attention transformer for survival prediction in gigapixel whole slide images. In *Proceedings of the IEEE/CVF International Conference on Computer Vision*, pp. 4015–4025, 2021b.

- Richard J Chen, Ming Y Lu, Drew FK Williamson, Tiffany Y Chen, Jana Lipkova, Muhammad Shaban, Maha Shady, Mane Williams, Bumjin Joo, Zahra Noor, et al. Pan-cancer integrative histology-genomic analysis via interpretable multimodal deep learning. arXiv preprint arXiv:2108.02278, 2021c.
- Richard J Chen, Chengkuan Chen, Yicong Li, Tiffany Y Chen, Andrew D Trister, Rahul G Krishnan, and Faisal Mahmood. Scaling vision transformers to gigapixel images via hierarchical self-supervised learning. In Proceedings of the IEEE/CVF Conference on Computer Vision and Pattern Recognition, pp. 16144–16155, 2022a.
- Richard J Chen, Ming Y Lu, Drew FK Williamson, Tiffany Y Chen, Jana Lipkova, Zahra Noor, Muhammad Shaban, Maha Shady, Mane Williams, Bumjin Joo, et al. Pan-cancer integrative histology-genomic analysis via multimodal deep learning. Cancer Cell, 40(8):865–878, 2022b.
- Zitian Chen, Yikang Shen, Mingyu Ding, Zhenfang Chen, Hengshuang Zhao, Erik G. Learned-Miller, and Chuang Gan. Mod-squad: Designing mixtures of experts as modular multi-task learners. In Proceedings of the IEEE/CVF Conference on Computer Vision and Pattern Recognition (CVPR), pp. 11828–11837, June 2023.
- Zewen Chi, Li Dong, Shaohan Huang, Damai Dai, Shuming Ma, Barun Patra, Saksham Singhal, Payal Bajaj, Xia Song, Xian-Ling Mao, et al. On the representation collapse of sparse mixture of experts. Advances in Neural Information Processing Systems, 35:34600–34613, 2022.
- Elisabeth B Claus, Neil Risch, and W Douglas Thompson. Genetic analysis of breast cancer in the cancer and steroid hormone study. American journal of human genetics, 48(2):232, 1991.
- Nicolas Coudray, Paolo Santiago Ocampo, Theodore Sakellaropoulos, Navneet Narula, Matija Snuderl, David Fenyö, Andre L Moreira, Narges Razavian, and Aristotelis Tsirigos. Classification and mutation prediction from non-small cell lung cancer histopathology images using deep learning. Nature medicine, 24(10):1559–1567, 2018.
- Yong Dai, Duyu Tang, Liangxin Liu, Minghuan Tan, Cong Zhou, Jingquan Wang, Zhangyin Feng, Fan Zhang, Xueyu Hu, and Shuming Shi. One model, multiple modalities: A sparsely activated approach for text, sound, image, video and code. CoRR, abs/2205.06126, 2022. doi: 10.48550/arXiv.2205.06126. URL <https://doi.org/10.48550/arXiv.2205.06126>.
- Alexey Dosovitskiy, Lucas Beyer, Alexander Kolesnikov, Dirk Weissenborn, Xiaohua Zhai, Thomas Unterthiner, Mostafa Dehghani, Matthias Minderer, Georg Heigold, Sylvain Gelly, et al. An image is worth 16x16 words: Transformers for image recognition at scale. arXiv preprint arXiv:2010.11929, 2020.
- Amelie Echle, Niklas Timon Rindtorff, Titus Josef Brinker, Tom Luedde, Alexander Thomas Pearson, and Jakob Nikolas Kather. Deep learning in cancer pathology: a new generation of clinical biomarkers. British journal of cancer, 124(4):686–696, 2021.
- David Eigen, Marc’Aurelio Ranzato, and Ilya Sutskever. Learning factored representations in a deep mixture of experts. arXiv preprint arXiv:1312.4314, 2013.
- Zhiwen Fan, Rishov Sarkar, Ziyu Jiang, Tianlong Chen, Kai Zou, Yu Cheng, Cong Hao, Zhangyang Wang, et al. M³vit: Mixture-of-experts vision transformer for efficient multi-task learning with model-accelerator co-design. Advances in Neural Information Processing Systems, 35:28441–28457, 2022.
- William Fedus, Barret Zoph, and Noam Shazeer. Switch transformers: Scaling to trillion parameter models with simple and efficient sparsity. The Journal of Machine Learning Research, 23(1):5232–5270, 2022.
- Francoise Galateau-Salle, Andrew Churg, Victor Roggli, William D Travis, World Health Organization Committee for Tumors, et al. The 2015 world health organization classification of tumors of the pleura: advances since the 2004 classification. Journal of thoracic oncology, 11(2):142–154, 2016.

- Yunhe Gao, Mu Zhou, and Dimitris N Metaxas. Utnet: a hybrid transformer architecture for medical image segmentation. In Medical Image Computing and Computer Assisted Intervention–MICCAI 2021: 24th International Conference, Strasbourg, France, September 27–October 1, 2021, Proceedings, Part III 24, pp. 61–71. Springer, 2021.
- Emily Gobin, Kayla Bagwell, John Wagner, David Mysona, Sharmila Sandirasegarane, Nathan Smith, Shan Bai, Ashok Sharma, Robert Schleifer, and Jin-Xiong She. A pan-cancer perspective of matrix metalloproteases (mmp) gene expression profile and their diagnostic/prognostic potential. BMC cancer, 19: 1–10, 2019.
- Sam Gross, Marc’Aurelio Ranzato, and Arthur Szlam. Hard mixtures of experts for large scale weakly supervised vision. In Proceedings of the IEEE Conference on Computer Vision and Pattern Recognition, pp. 6865–6873, 2017.
- Jie Hao, Sai Chandra Kosaraju, Nelson Zange Tsaku, Dae Hyun Song, and Mingon Kang. Page-net: interpretable and integrative deep learning for survival analysis using histopathological images and genomic data. In Pacific Symposium on Biocomputing 2020, pp. 355–366. World Scientific, 2019.
- Frank E Harrell, Robert M Califf, David B Pryor, Kerry L Lee, and Robert A Rosati. Evaluating the yield of medical tests. Jama, 247(18):2543–2546, 1982.
- Simon Haykin. Neural networks: a comprehensive foundation. Prentice Hall PTR, 1998.
- Hussein Hazimeh, Zhe Zhao, Aakanksha Chowdhery, Maheswaran Sathiamoorthy, Yihua Chen, Rahul Mazumder, Lichan Hong, and Ed H. Chi. Dselect-k: Differentiable selection in the mixture of experts with applications to multi-task learning. In Marc’Aurelio Ranzato, Alina Beygelzimer, Yann N. Dauphin, Percy Liang, and Jennifer Wortman Vaughan (eds.), Advances in Neural Information Processing Systems 34: Annual Conference on Neural Information Processing Systems 2021, NeurIPS 2021, December 6-14, 2021, virtual, pp. 29335–29347, 2021. URL <https://proceedings.neurips.cc/paper/2021/hash/f5ac21cd0ef1b88e9848571aeb53551a-Abstract.html>.
- Along He, Kai Wang, Tao Li, Chengkun Du, Shuang Xia, and Huazhu Fu. H2former: An efficient hierarchical hybrid transformer for medical image segmentation. IEEE Transactions on Medical Imaging, 2023.
- Andreas Heindl, Sidra Nawaz, and Yinyin Yuan. Mapping spatial heterogeneity in the tumor microenvironment: a new era for digital pathology. Laboratory investigation, 95(4):377–384, 2015.
- Jiaxin Hou, Xiaoqi Jia, Yaoqin Xie, and Wenjian Qin. Integrative histology-genomic analysis predicts hepatocellular carcinoma prognosis using deep learning. Genes, 13(10):1770, 2022.
- Hanyao Huang, Ou Zheng, Dongdong Wang, Jiayi Yin, Zijin Wang, Shengxuan Ding, Heng Yin, Chuan Xu, Renjie Yang, Qian Zheng, et al. Chatgpt for shaping the future of dentistry: the potential of multi-modal large language model. International Journal of Oral Science, 15(1):29, 2023.
- Maximilian Ilse, Jakub Tomczak, and Max Welling. Attention-based deep multiple instance learning. In International conference on machine learning, pp. 2127–2136. PMLR, 2018.
- Guillaume Jaume, Anurag Vaidya, Richard Chen, Drew Williamson, Paul Liang, and Faisal Mahmood. Modeling dense multimodal interactions between biological pathways and histology for survival prediction. arXiv preprint arXiv:2304.06819, 2023.
- Hao Jiang, Ke Zhan, Jianwei Qu, Yongkang Wu, Zhaoye Fei, Xinyu Zhang, Lei Chen, Zhicheng Dou, Xipeng Qiu, Zikai Guo, et al. Towards more effective and economic sparsely-activated model. arXiv preprint arXiv:2110.07431, 2021.
- Shivam Kalra, Hamid R Tizhoosh, Sultaan Shah, Charles Choi, Savvas Damaskinos, Amir Safarpour, Sobhan Shafiei, Morteza Babaie, Phedias Diamandis, Clinton JV Campbell, et al. Pan-cancer diagnostic consensus through searching archival histopathology images using artificial intelligence. NPJ digital medicine, 3(1): 31, 2020.

- Rick Kamps, Rita D Brandão, Bianca J van den Bosch, Aimee DC Paulussen, Sofia Xanthoulea, Marinus J Blok, and Andrea Romano. Next-generation sequencing in oncology: genetic diagnosis, risk prediction and cancer classification. *International journal of molecular sciences*, 18(2):308, 2017.
- Jakob Nikolas Kather, Meggy Suarez-Carmona, Pornpimol Charoentong, Cleo-Aron Weis, Daniela Hirsch, Peter Bankhead, Marcel Horning, Dyke Ferber, Ivan Kel, Esther Herpel, et al. Topography of cancer-associated immune cells in human solid tumors. *Elife*, 7:e36967, 2018.
- Jakob Nikolas Kather, Alexander T Pearson, Niels Halama, Dirk Jäger, Jeremias Krause, Sven H Loosen, Alexander Marx, Peter Boor, Frank Tacke, Ulf Peter Neumann, et al. Deep learning can predict microsatellite instability directly from histology in gastrointestinal cancer. *Nature medicine*, 25(7):1054–1056, 2019.
- Young-Gon Kim, In Hye Song, Hyunna Lee, Sungchul Kim, Dong Hyun Yang, Namkug Kim, Dongho Shin, Yeonsoo Yoo, Kywoon Lee, Dahye Kim, et al. Challenge for diagnostic assessment of deep learning algorithm for metastases classification in sentinel lymph nodes on frozen tissue section digital slides in women with breast cancer. *Cancer Research and Treatment: Official Journal of Korean Cancer Association*, 52(4):1103–1111, 2020.
- Young Jin Kim, Ammar Ahmad Awan, Alexandre Muzio, Andrés Felipe Cruz-Salinas, Liyang Lu, Amr Hendy, Samyam Rajbhandari, Yuxiong He, and Hany Hassan Awadalla. Scalable and efficient moe training for multitask multilingual models. *CoRR*, abs/2109.10465, 2021a. URL <https://arxiv.org/abs/2109.10465>.
- Young Jin Kim, Ammar Ahmad Awan, Alexandre Muzio, Andres Felipe Cruz Salinas, Liyang Lu, Amr Hendy, Samyam Rajbhandari, Yuxiong He, and Hany Hassan Awadalla. Scalable and efficient moe training for multitask multilingual models. *arXiv preprint arXiv:2109.10465*, 2021b.
- Günter Klambauer, Thomas Unterthiner, Andreas Mayr, and Sepp Hochreiter. Self-normalizing neural networks. *Advances in neural information processing systems*, 30, 2017.
- Zhenglun Kong, Peiyan Dong, Xiaolong Ma, Xin Meng, Mengshu Sun, Wei Niu, Xuan Shen, Geng Yuan, Bin Ren, Minghai Qin, et al. Spvit: Enabling faster vision transformers via soft token pruning. *arXiv preprint arXiv:2112.13890*, 2021.
- Zhenglun Kong, Haoyu Ma, Geng Yuan, Mengshu Sun, Yanyue Xie, Peiyan Dong, Xin Meng, Xuan Shen, Hao Tang, Minghai Qin, et al. Peeling the onion: Hierarchical reduction of data redundancy for efficient vision transformer training. In *Proceedings of the AAAI Conference on Artificial Intelligence*, volume 37, pp. 8360–8368, 2023.
- Martin Kreutz, Maik Anschütz, Stefan Gehlen, Thorsten Grünendick, and Klaus Hoffmann. Automated diagnosis of skin cancer using digital image processing and mixture-of-experts. In *Bildverarbeitung für die Medizin 2001: Algorithmen—Systeme—Anwendungen*, pp. 357–361. Springer, 2001.
- Sneha Kudugunta, Yanping Huang, Ankur Bapna, Maxim Krikun, Dmitry Lepikhin, Minh-Thang Luong, and Orhan Firat. Beyond distillation: Task-level mixture-of-experts for efficient inference. In Marie-Francine Moens, Xuanjing Huang, Lucia Specia, and Scott Wen-tau Yih (eds.), *Findings of the Association for Computational Linguistics: EMNLP 2021, Virtual Event / Punta Cana, Dominican Republic, 16-20 November, 2021*, pp. 3577–3599. Association for Computational Linguistics, 2021. doi: 10.18653/v1/2021.findings-emnlp.304. URL <https://doi.org/10.18653/v1/2021.findings-emnlp.304>.
- Dana Lahat, Tülay Adalı, and Christian Jutten. Multimodal data fusion: an overview of methods, challenges, and prospects. *Proceedings of the IEEE*, 103(9):1449–1477, 2015.
- Dmitry Lepikhin, HyoukJoong Lee, Yuanzhong Xu, Dehao Chen, Orhan Firat, Yanping Huang, Maxim Krikun, Noam Shazeer, and Zhifeng Chen. Gshard: Scaling giant models with conditional computation and automatic sharding. *arXiv preprint arXiv:2006.16668*, 2020.
- Hang Li, Fan Yang, Xiaohan Xing, Yu Zhao, Jun Zhang, Yueping Liu, Mengxue Han, Junzhou Huang, Liansheng Wang, and Jianhua Yao. Multi-modal multi-instance learning using weakly correlated histopathological images and tabular clinical information. In *International Conference on Medical Image Computing and Computer-Assisted Intervention*, pp. 529–539. Springer, 2021.

- Ruiqing Li, Xingqi Wu, Ao Li, and Minghui Wang. Hfbsurv: hierarchical multimodal fusion with factorized bilinear models for cancer survival prediction. Bioinformatics, 38(9):2587–2594, 2022.
- Yuxuan Lou, Fuzhao Xue, Zangwei Zheng, and Yang You. Cross-token modeling with conditional computation. arXiv preprint arXiv:2109.02008, 2021.
- Ming Y Lu, Drew FK Williamson, Tiffany Y Chen, Richard J Chen, Matteo Barbieri, and Faisal Mahmood. Data-efficient and weakly supervised computational pathology on whole-slide images. Nature biomedical engineering, 5(6):555–570, 2021.
- Ming Y Lu, Richard J Chen, Dehan Kong, Jana Lipkova, Rajendra Singh, Drew FK Williamson, Tiffany Y Chen, and Faisal Mahmood. Federated learning for computational pathology on gigapixel whole slide images. Medical image analysis, 76:102298, 2022.
- Jiaqi Ma, Zhe Zhao, Xinyang Yi, Jilin Chen, Lichan Hong, and Ed H. Chi. Modeling task relationships in multi-task learning with multi-gate mixture-of-experts. In Yike Guo and Faisal Farooq (eds.), Proceedings of the 24th ACM SIGKDD International Conference on Knowledge Discovery & Data Mining, KDD 2018, London, UK, August 19-23, 2018, pp. 1930–1939. ACM, 2018. doi: 10.1145/3219819.3220007. URL <https://doi.org/10.1145/3219819.3220007>.
- Andriy Marusyk and Kornelia Polyak. Tumor heterogeneity: causes and consequences. Biochimica et Biophysica Acta (BBA)-Reviews on Cancer, 1805(1):105–117, 2010.
- Andriy Marusyk, Vanessa Almendro, and Kornelia Polyak. Intra-tumour heterogeneity: a looking glass for cancer? Nature reviews cancer, 12(5):323–334, 2012.
- Manasi K Mayekar and Trever G Bivona. Current landscape of targeted therapy in lung cancer. Clinical Pharmacology & Therapeutics, 102(5):757–764, 2017.
- Paul Michel, Omer Levy, and Graham Neubig. Are sixteen heads really better than one? Advances in neural information processing systems, 32, 2019.
- Pooya Mobadersany, Safoora Yousefi, Mohamed Amgad, David A Gutman, Jill S Barnholtz-Sloan, José E Velázquez Vega, Daniel J Brat, and Lee AD Cooper. Predicting cancer outcomes from histology and genomics using convolutional networks. Proceedings of the National Academy of Sciences, 115(13):E2970–E2979, 2018.
- Ghulam Muhammad, Fatima Alshehri, Fakhri Karray, Abdulmotaleb El Saddik, Mansour Alsulaiman, and Tiago H Falk. A comprehensive survey on multimodal medical signals fusion for smart healthcare systems. Information Fusion, 76:355–375, 2021.
- Basil Mustafa, Carlos Riquelme, Joan Puigcerver, Rodolphe Jenatton, and Neil Houlsby. Multimodal contrastive learning with limoe: the language-image mixture of experts. Advances in Neural Information Processing Systems, 35:9564–9576, 2022.
- Sungmin Myoung. Modified mixture of experts for the diagnosis of perfusion magnetic resonance imaging measures in locally rectal cancer patients. Healthcare Informatics Research, 19(2):130–136, 2013.
- Rachael Natrajan, Heba Sailem, Faraz K Mardakheh, Mar Arias Garcia, Christopher J Tape, Mitch Dowsett, Chris Bakal, and Yinyin Yuan. Microenvironmental heterogeneity parallels breast cancer progression: a histology–genomic integration analysis. PLoS medicine, 13(2):e1001961, 2016.
- Jiquan Ngiam, Aditya Khosla, Mingyu Kim, Juhan Nam, Honglak Lee, and Andrew Y Ng. Multimodal deep learning. In Proceedings of the 28th international conference on machine learning (ICML-11), pp. 689–696, 2011.
- Svetlana Pavlitskaya, Christian Hubschneider, Michael Weber, Ruby Moritz, Fabian Huger, Peter Schlicht, and Marius Zollner. Using mixture of expert models to gain insights into semantic segmentation. In Proceedings of the IEEE/CVF Conference on Computer Vision and Pattern Recognition Workshops, pp. 342–343, 2020.

- Sudhir Raman, Thomas J Fuchs, Peter J Wild, Edgar Dahl, Joachim M Buhmann, and Volker Roth. Infinite mixture-of-experts model for sparse survival regression with application to breast cancer. BMC bioinformatics, 11:1–10, 2010.
- Aditya Ramesh, Prafulla Dhariwal, Alex Nichol, Casey Chu, and Mark Chen. Hierarchical text-conditional image generation with CLIP latents. CoRR, abs/2204.06125, 2022. doi: 10.48550/arXiv.2204.06125. URL <https://doi.org/10.48550/arXiv.2204.06125>.
- Yongming Rao, Wenliang Zhao, Benlin Liu, Jiwen Lu, Jie Zhou, and Cho-Jui Hsieh. Dynamicvit: Efficient vision transformers with dynamic token sparsification. Advances in neural information processing systems, 34:13937–13949, 2021.
- Carlos Riquelme, Joan Puigcerver, Basil Mustafa, Maxim Neumann, Rodolphe Jenatton, André Susano Pinto, Daniel Keysers, and Neil Houlsby. Scaling vision with sparse mixture of experts. Advances in Neural Information Processing Systems, 34:8583–8595, 2021.
- Chitwan Saharia, William Chan, Saurabh Saxena, Lala Li, Jay Whang, Emily L. Denton, Seyed Kamyar Seyed Ghasemipour, Raphael Gontijo Lopes, Burcu Karagol Ayan, Tim Salimans, Jonathan Ho, David J. Fleet, and Mohammad Norouzi. Photorealistic text-to-image diffusion models with deep language understanding. In NeurIPS, 2022. URL http://papers.nips.cc/paper_files/paper/2022/hash/ec795aeadae0b7d230fa35cbaf04c041-Abstract-Conference.html.
- E Sala, E Mema, Y Himoto, H Veeraraghavan, JD Brenton, A Snyder, B Weigelt, and HA Vargas. Unravelling tumour heterogeneity using next-generation imaging: radiomics, radiogenomics, and habitat imaging. Clinical radiology, 72(1):3–10, 2017.
- Muhammad Shaban, Syed Ali Khurram, Muhammad Moazam Fraz, Najah Alsubaie, Iqra Masood, Sajid Mushtaq, Mariam Hassan, Asif Loya, and Nasir M Rajpoot. A novel digital score for abundance of tumour infiltrating lymphocytes predicts disease free survival in oral squamous cell carcinoma. Scientific reports, 9(1):13341, 2019.
- Daryoush Shahbazi-Gahrouei, Pegah Moradi Khaniabadi, Bita Moradi Khaniabadi, and Saghar Shahbazi-Gahrouei. Medical imaging modalities using nanoprobe for cancer diagnosis: A literature review on recent findings. Journal of research in medical sciences: the official journal of Isfahan University of Medical Sciences, 24, 2019.
- Zhuchen Shao, Hao Bian, Yang Chen, Yifeng Wang, Jian Zhang, Xiangyang Ji, et al. Transmil: Transformer based correlated multiple instance learning for whole slide image classification. Advances in neural information processing systems, 34:2136–2147, 2021.
- Zhuchen Shao, Yang Chen, Hao Bian, Jian Zhang, Guojun Liu, and Yongbing Zhang. HvtSurv: hierarchical vision transformer for patient-level survival prediction from whole slide image. In Proceedings of the AAAI Conference on Artificial Intelligence, volume 37, pp. 2209–2217, 2023.
- Noam Shazeer, Azalia Mirhoseini, Krzysztof Maziarz, Andy Davis, Quoc Le, Geoffrey Hinton, and Jeff Dean. Outrageously large neural networks: The sparsely-gated mixture-of-experts layer. arXiv preprint arXiv:1701.06538, 2017a.
- Noam Shazeer, Azalia Mirhoseini, Krzysztof Maziarz, Andy Davis, Quoc V. Le, Geoffrey E. Hinton, and Jeff Dean. Outrageously large neural networks: The sparsely-gated mixture-of-experts layer. In 5th International Conference on Learning Representations, ICLR 2017, Toulon, France, April 24-26, 2017, Conference Track Proceedings. OpenReview.net, 2017b.
- Dai Shimizu, Kenzui Taniue, Yusuke Matsui, Hiroshi Haeno, Hiromitsu Araki, Fumihito Miura, Mitsuko Fukunaga, Kenji Shiraishi, Yuji Miyamoto, Seiichi Tsukamoto, et al. Pan-cancer methylome analysis for cancer diagnosis and classification of cancer cell of origin. Cancer Gene Therapy, 29(5):428–436, 2022.

- Velmurugan Subbiah Parvathy, Sivakumar Pothiraj, and Jenyfal Sampson. A novel approach in multimodality medical image fusion using optimal shearlet and deep learning. International Journal of Imaging Systems and Technology, 30(4):847–859, 2020.
- Vaishnavi Subramanian, Benjamin Chidester, Jian Ma, and Minh N Do. Correlating cellular features with gene expression using cca. In 2018 IEEE 15th International Symposium on Biomedical Imaging (ISBI 2018), pp. 805–808. IEEE, 2018.
- Harini Suresh, Nathan Hunt, Alistair Johnson, Leo Anthony Celi, Peter Szolovits, and Marzyeh Ghassemi. Clinical intervention prediction and understanding with deep neural networks. In Machine Learning for Healthcare Conference, pp. 322–337. PMLR, 2017.
- Paolo Tarantino, Luca Mazzarella, Antonio Marra, Dario Trapani, and Giuseppe Curigliano. The evolving paradigm of biomarker actionability: histology-agnosticism as a spectrum, rather than a binary quality. Cancer Treatment Reviews, 94:102169, 2021.
- Avnesh S Thakor and Sanjiv S Gambhir. Nanooncology: the future of cancer diagnosis and therapy. CA: a cancer journal for clinicians, 63(6):395–418, 2013.
- Elif Derya Übeyli. A mixture of experts network structure for breast cancer diagnosis. Journal of medical systems, 29(5):569–579, 2005.
- Ashish Vaswani, Noam Shazeer, Niki Parmar, Jakob Uszkoreit, Llion Jones, Aidan N Gomez, Łukasz Kaiser, and Illia Polosukhin. Attention is all you need. Advances in neural information processing systems, 30, 2017.
- Xin Wang, Fisher Yu, Lisa Dunlap, Yi-An Ma, Ruth Wang, Azalia Mirhoseini, Trevor Darrell, and Joseph E Gonzalez. Deep mixture of experts via shallow embedding. In Uncertainty in artificial intelligence, pp. 552–562. PMLR, 2020.
- Zhikang Wang, Qian Gao, Xiaoping Yi, Xinyu Zhang, Yiwen Zhang, Daokun Zhang, Pietro Liò, Chris Bain, Richard Bessed, Shanshan Li, et al. Surformer: An interpretable pattern-perceptive survival transformer for cancer survival prediction from histopathology whole slide images. Computer Methods and Programs in Biomedicine, 241:107733, 2023.
- Zhiqin Wang, Ruiqing Li, Minghui Wang, and Ao Li. Gpdbn: deep bilinear network integrating both genomic data and pathological images for breast cancer prognosis prediction. Bioinformatics, 37(18):2963–2970, 2021.
- Haiying Xia, Richeng Lan, Haisheng Li, and Shuxiang Song. ST-VQA: shrinkage transformer with accurate alignment for visual question answering. Appl. Intell., 53(18):20967–20978, 2023. doi: 10.1007/s10489-023-04564-x. URL <https://doi.org/10.1007/s10489-023-04564-x>.
- Yunyang Xiong, Zhanpeng Zeng, Rudrasis Chakraborty, Mingxing Tan, Glenn Fung, Yin Li, and Vikas Singh. Nyströmformer: A nyström-based algorithm for approximating self-attention. In Proceedings of the AAAI Conference on Artificial Intelligence, volume 35, pp. 14138–14148, 2021.
- Nozomu Yanaihara, Natasha Caplen, Elise Bowman, Masahiro Seike, Kensuke Kumamoto, Ming Yi, Robert M Stephens, Aikou Okamoto, Jun Yokota, Tadao Tanaka, et al. Unique microrna molecular profiles in lung cancer diagnosis and prognosis. Cancer cell, 9(3):189–198, 2006.
- Jiawen Yao, Xinliang Zhu, Jitendra Jonnagaddala, Nicholas Hawkins, and Junzhou Huang. Whole slide images based cancer survival prediction using attention guided deep multiple instance learning networks. Medical Image Analysis, 65:101789, 2020.
- Hanrong Ye and Dan Xu. Taskexpert: Dynamically assembling multi-task representations with memorial mixture-of-experts. CoRR, abs/2307.15324, 2023.
- Yuhui Yuan, Rao Fu, Lang Huang, Weihong Lin, Chao Zhang, Xilin Chen, and Jingdong Wang. Hrformer: High-resolution transformer for dense prediction. arXiv preprint arXiv:2110.09408, 2021.

- Hongrun Zhang, Yanda Meng, Yitian Zhao, Yihong Qiao, Xiaoyun Yang, Sarah E Coupland, and Yalin Zheng. Dtf-d-mil: Double-tier feature distillation multiple instance learning for histopathology whole slide image classification. In Proceedings of the IEEE/CVF Conference on Computer Vision and Pattern Recognition, pp. 18802–18812, 2022.
- Zhengyan Zhang, Yankai Lin, Zhiyuan Liu, Peng Li, Maosong Sun, and Jie Zhou. Moefication: Transformer feed-forward layers are mixtures of experts. arXiv preprint arXiv:2110.01786, 2021.
- Fengtao Zhou and Hao Chen. Cross-modal translation and alignment for survival analysis. In Proceedings of the IEEE/CVF International Conference on Computer Vision, pp. 21485–21494, 2023.
- Yanqi Zhou, Tao Lei, Hanxiao Liu, Nan Du, Yanping Huang, Vincent Zhao, Andrew M Dai, Quoc V Le, James Laudon, et al. Mixture-of-experts with expert choice routing. Advances in Neural Information Processing Systems, 35:7103–7114, 2022.
- Jinguo Zhu, Xizhou Zhu, Wenhai Wang, Xiaohua Wang, Hongsheng Li, Xiaogang Wang, and Jifeng Dai. Uni-perceiver-moe: Learning sparse generalist models with conditional moes. Advances in Neural Information Processing Systems, 35:2664–2678, 2022a.
- Rui Zhu, Xiongfei Li, Sa Huang, and Xiaoli Zhang. Multimodal medical image fusion using adaptive co-occurrence filter-based decomposition optimization model. Bioinformatics, 38(3):818–826, 2022b.
- Simiao Zuo, Xiaodong Liu, Jian Jiao, Young Jin Kim, Hany Hassan, Ruofei Zhang, Tuo Zhao, and Jianfeng Gao. Taming sparsely activated transformer with stochastic experts. arXiv preprint arXiv:2110.04260, 2021.

This is the supplementary material for One Leaf Knows Autumn: A Piece of Data-Model Facilitates Efficient Cancer Prognosis with Histological and Genomic Modalities.

We provide the following materials in this manuscript:

- Sec. A the details of datasets and baselines.
- Sec. B the title explanation.

A Datasets and Baseline Details

Datasets Details We have utilized data from 12 public cancer types sourced from The Cancer Genome Atlas (TCGA) Program for our experiments. These cancer types include Bladder Urothelial Carcinoma (BLCA), Breast Invasive Carcinoma (BRCA), Head and Neck Squamous Cell Carcinoma (HNSC), Kidney Renal Clear Cell Carcinoma (KIRC), Kidney Renal Papillary Cell Carcinoma (KIRP), Liver Hepatocellular Carcinoma (LIHC), Lung Adenocarcinoma (LUAD), Lung Squamous Cell Carcinoma (LUSC), Pancreatic Adenocarcinoma (PAAD), Skin Cutaneous Melanoma (SKCM), Stomach Adenocarcinoma (STAD), and Uterine Corpus Endometrial Carcinoma (UCEC), totally involving hundreds of patients and Hematoxylin and Eosin (H&E) diagnostic Whole Slide Images (WSIs). The elaborate information regarding these datasets is provided in Table 9. Thousands of genomic features are compiled for each patient, sourced from Copy Number Variation (CNV) data, mutation status, and bulk RNA-Seq expression derived from the differentially expressed genes. This data is collected from The Cancer Genome Atlas (TCGA) and the cBioPortal Cerami et al. (2012).

Baseline Details. To facilitate a thorough comparison, we implement and assess various survival prediction methods using the same 5-fold cross-validation splits. These methods encompass both the single-modal learning paradigm and the multi-modal learning paradigm. The experimental results for all these methods across the 12 TCGA datasets are summarized in Table 1. The Params and FLOPs of **CancerMoE** and all baseline methods are calculated on the **BRCA** dataset. For feature extraction, once segmentation is completed, image patches of dimensions 256×256 are extracted without overlapping, based on the $20\times$ equivalent pyramid level from all identified tissue regions. Following this, a pre-trained ResNet50 model, which had been trained on Imagenet, is employed as an encoder. It converted each 256×256 patch into a 1024-dimensional feature vector using spatial average pooling after the third residual block.

Baseline Modal. Machine learning models: 1) SNN Klambauer et al. (2017): It is a self-normalizing network model, which serves as the single-modal baseline when working exclusively with genomic profiles. 2) OmicMLP Haykin (1998); Jaume et al. (2023): It utilizes a 4-layer Multi-Layer Perceptron (MLP). 3) AttnMISL Ilse et al. (2018): It employs gated-attention pooling for the WSIs. 4) Patch-GCN Chen et al. (2021a): It explores a hierarchical aggregation approach to consolidate image-level features. 5) TransMIL Shao et al. (2021): TransMIL approximates patch self-attention using the Nyström method Xiong et al. (2021). 6) MCAT Chen et al. (2021b): MCAT employs Genomic-Guided Co-Attention (GCA), a mechanism similar to the standard transformer attention that serves the purpose of establishing relationships between image-grid data and word embeddings, much like in the context of VQA Vaswani et al. (2017). Biology literature-based methods: 1) PorpoiseAMIL Chen et al. (2022b): It is mainly based on the attention module, projection, and prediction layers. 2) CLAM-SB and CLAM-MB Lu et al. (2021): After segmentation of WSIs using Clustering-constrained Attention Multiple (CLAM) instance learning’s method Lu et al. (2021), survival prediction is performed in two ways. 3) MMF Chen et al. (2022b): An approach is taken to incorporate a multimodal fusion layer, an extension of Pathomic Fusion Chen et al. (2020), to merge the features from SNN and PorpoiseAMIL.

B Title Explanation

One Leaf Knows Autumn Generally, the passage of time can be likened to the shifting seasons of the year, each akin to a chapter in the story of one’s life. For cancer patients, their journey can often mirror the autumn season, a stage marked by the undeniable symbols of harvest and beauty but one that quickly gives way to the withered chill of winter. In the face of this challenging transition, our mission is to offer patients a

Table 9: TCGA 12 Cancers Case number and Feature Summary.

Cancer	WSIs	Genomics Profile
BLCA	437	20404
BRCA	1021	20980
HNSC	437	2217
KIRC	350	2513
KIRP	284	1587
LIHC	346	2583
LUAD	515	21155
LUSC	484	2416
PAAD	180	1659
SKCM	268	2350
STAD	372	2543
UCEC	539	9081

glimpse of tackling the impending autumn through a small leaf to help them prepare for the seasons ahead. We aim to usher in the early awareness of autumn in the lives of cancer patients. By equipping with our methods, we can provide better support during the autumn phase of their prognosis, extending the chapters of happiness in their lives. This is the meaning of One Leaf Knows Autumn: to use the most critical parts of histopathology images and genetic signatures to help cancer patients with better treatment and prognosis.